Environ. Sci. Technol. **2002**, *36,* 976−981

Arsenic(III) Oxidation and Arsenic(V) Adsorption Reactions on Synthetic Birnessite

BRUCE A. MANNING,*,† SCOTT E. FENDORF,‡ BENJAMIN BOSTICK,‡ AND DONALD L. SUAREZ§

Department of Chemistry and Biochemistry, San Francisco State University, San Francisco, California 94132, Department of Geological and Environmental Sciences, Stanford University, Palo Alto, California 94305, and USDA-ARS U.S. Salinity Laboratory, 450 West Big Springs Road, Riverside, California 92507

The oxidation of arsenite (As(III)) by manganese oxide is an important reaction in both the natural cycling of As and the development of remediation technology for lowering the concentration of dissolved As(III) in drinking water. This study used both a conventional stirred reaction apparatus and extended X-ray absorption fine structure (EXAFS) spectroscopy to investigate the reactions of As(III) and As(V) with synthetic birnessite (MnO_2). Stirred reactor experiments indicate that As(III) is oxidized by MnO_2 followed by the adsorption of the As(V) reaction product on the MnO_2 solid phase. The As(V)−Mn interatomic distance determined by EXAFS analysis for both As(III)- and As(V)-treated MnO_2 was 3.22 Å, giving evidence for the formation of As(V) adsorption complexes on MnO_2 crystallite surfaces. The most likely As(V)−MnO_2 complex is a bidentate binuclear corner sharing (bridged) complex occurring at MnO_2 crystallite edges and interlayer domains. In the As(III)-treated MnO_2 systems, reductive dissolution of the MnO_2 solid during the oxidation of As(III) caused an increase in the adsorption of As(V) when compared with As(V)-treated MnO_2. This suggested that As(III) oxidation caused a surface alteration, creating fresh reaction sites for As(V) on MnO_2 surfaces.

Introduction

The environmental and human health impacts of elevated concentrations of As in groundwater have received increased attention because of its toxicity (*1*−*3*). The predominant forms of As in soil and water are as inorganic arsenate (As(V)) and arsenite (As(III)) (*4*−*7*). Under oxidizing and aerobic conditions, the As(V) species predominates and exists as oxyanions of arsenic acid ($H_2AsO_4^-$ and $HAsO_4^{2-}$) (*8*). The As(III) species exists as undissociated arsenious acid ($H_3AsO_3^0$) below pH 9.2 (*9*) and predominates under reducing conditions in sediments, groundwater, and soils (*8*−*11*). The As(III) species is substantially more toxic than As(V) (*12*, *13*) and tends to be more weakly bound to soils than As(V). This latter phenomenon is probably due to a combination of factors, including concomitant reductive dissolution of Fe oxides which adsorb both As(III) and As(V) and the tendency for As(III) to adsorb more weakly to most aluminum oxide and aluminosilicate soil minerals than As(V) (*14*, *15*).

An important reaction in the environmental fate of As(III) is heterogeneous oxidation on soil mineral surfaces (*16*−*21*). Manganese oxides are extremely important minerals because they readily oxidize many reduced species such as As(III) (*18*−*24*), Co(II) (*25*, *26*), Cr(III) (*27*), and organic molecules (*28*, *29*). The crystalline structures of Mn oxides are of environmental interest because of the adsorptive and oxidative capabilities of these minerals. Synthetic birnessite has been extensively investigated because it is representative of many naturally occurring manganese oxide materials (*18*−*21*, *25*, *30*, *31*). The Na- and K-substituted birnessite are phyllomanganates, possessing layered sheet structures with edge-sharing Mn octahedra (*25*, *30*). These materials have been described as nearly vacancy-free layers of Mn octahedra influenced by Jahn−Teller distortion when Mn(III) substitutes for Mn(IV). An ordered distribution of Mn(III)-rich rows, interlayer counterions (Na^+ or K^+), and octahedral vacancies completes the crystal structure (*25*, *30*). The average chemical formula for sodium birnessite has been given as $Na_{0.333}(Mn^{4+}_{0.722}\ Mn^{3+}_{0.222}\ Mn^{2+}_{0.055})O_2$ (*30*), indicating a partial negative charge per unit cell. Moore et al. (*18*) showed that the O/Mn ratio for most synthetic birnessites is near 2. For simplicity, the birnessite chemical formula will be simplified to MnO_2 in this paper.

Details about the chemical mechanism of As(III) heterogeneous oxidation by birnessite are emerging (*18*−*21*). Oxidation of As(III) by synthetic birnessite is coupled with the reductive dissolution of the MnO_2 surface and results in the release of both As(V) and Mn(II) to solution at low pH (*20*, *22*). The net stoichiometry of the reaction is

$$MnO_2 + H_3AsO_3 + 2H^+ = Mn^{2+} + H_3AsO_4 + H_2O \quad (1)$$

Recent work by Nesbitt et al. (*19*) using X-ray photoelectron spectroscopy (XPS) has shown that the oxidation of As(III) by the synthetic 7 Å birnessite surface proceeds by a two-step pathway, involving the reduction of Mn(IV) to Mn(III)

$$2MnO_2 + H_3AsO_3 = 2MnOOH^* + H_3AsO_4 \quad (2)$$

where MnOOH* is a Mn(III) intermediate reaction product. The reaction in eq 2 is followed by the reaction of As(III) with MnOOH*

$$2MnOOH^* + H_3AsO_3 + 4H^+ = 2Mn^{2+} + H_3AsO_4 + 3H_2O \quad (3)$$

An additional reaction could include the adsorption of As(V) by the MnO_2 surface

$$2Mn{-}OH + H_3AsO_4 = (MnO)_2AsOOH + 2H_2O \quad (4)$$

where Mn−OH represents a reactive hydroxyl group on the MnO_2 surface and $(MnO)_2AsOOH$ represents the As(V) surface complex. Though considerable effort has yielded mechanistic details about the reactions of As(III) with MnO_2 compounds, very little information is available about the formation of As(V) complexes after the oxidation of As(III).

To provide new insight into the reaction of As(III) with a representative Mn oxide, the objectives of this study were (1) to investigate the reactivity of As(III) with a synthetic MnO_2 compound, using a stirred reactor combined with an

* Corresponding author phone (415) 338-1292; fax: (415) 276-4759; e-mail: bmanning@sfsu.edu.
† San Francisco State University.
‡ Stanford University.
§ USDA-ARS U.S. Salinity Laboratory.

10.1021/es0110170 CCC: $22.00
Published on Web 01/31/2002

advanced technique for dissolved As(III)/As(V) speciation, and (2) to use EXAFS spectroscopy to examine the coordination environment of the surface complexes formed when As(III) and As(V) are reacted with MnO_2. This investigation was designed to link the findings of previous work (*18*−*21*) with new information derived from EXAFS spectroscopy.

Materials and Methods

Synthesis of MnO_2. Potassium birnessite, a 7 Å manganite, was synthesized following the procedures of McKenzie (*26*). Heated 0.4 M $KMnO_4$ was prepared in a 1 L glass separatory funnel with an outlet flow preset and clamped to deliver 950 mL/min. Another 250 mL separatory funnel containing heated (60 °C) concentrated HCl (Baker, Instrapure) with an outlet flow preset and clamped to deliver 66 mL/min was used. Mixing of the 0.4 M $KMnO_4$ with concentrated HCl was initiated by simultaneously unclamping the separatory funnels and collecting the resulting mixture in a 2.5 L glass beaker on a stirring hot plate heated at 90 °C in a fumehood. After stirring for an additional 10 min at 90 °C, the mixture was allowed to cool to room temperature (23 °C), transferred to 250 mL polycarbonate centrifuge bottles, and repeatedly rinsed with deionized (DI) water. After 10 rinse cycles the potassium concentration in the rinseate was analyzed by acetylene flame atomic absorption spectrometry (AAS) and was below 0.005 mM K. The MnO_2 solids were air-dried and gently crushed and sieved to pass a 100 μm sieve.

The synthetic MnO_2 was characterized by several methods, including the determination of the K content of the solid MnO_2, X-ray diffraction (XRD) analysis, and specific surface area. The K content was determined by dissolving 0.100 g of MnO_2 in 20 mL of 2.2 M H_2O_2/0.5 M HCl followed by flame AAS analysis. The specific surface area was determined by single-point Brunauer−Emmett−Teller (BET) N_2 adsorption using a Quantisorb Jr. flow-through surface area analyzer (Quantichrome Corp.). The crystallinity of the material was analyzed by powder X-ray diffraction analysis using Cu Kα radiation.

Reaction of As(III) with Synthetic MnO_2. The reaction of As(III) with MnO_2 was investigated using a rotating propeller-stirred reactor in a temperature controlled bath (22 °C). A 1 L glass beaker containing either 40 or 100 mg of synthetic MnO_2 and 400 mL of 0.10 M NaCl (100 or 250 mg L^{-1} MnO_2) was stirred and equilibrated for 1 h without gas atmospheric control. The pH of the suspensions was measured with a Corning semi-micro glass combination electrode and a Corning Ion Analyzer 150. For all experiments, the suspension pH was maintained at 6.50, which was near the ambient pH of the suspensions. A stock solution containing 13.33 mM As(III) was prepared by dissolving 0.867 g of $NaAsO_2$ (Sigma) in 500 mL of DI water.

The batch reaction was initiated by the addition of 3 mL of 13.33 mM As(III) to the suspension, making the solution 0.10 mM As(III). The reaction was monitored by filtration of 2 mL aliquots with 0.1 μm membranes and As(III)/As(V) speciation analysis by high-performance liquid chromatography atomic absorption spectrophotometry (HPLC−HGAAS) (*32*). This method separates As(III) and As(V) with a Dionex AS11 Ionpac anion exchange column in-line with a continuous flow-through hydride generator (Varian VGA 76) and a PerkinElmer 3030B AA spectrometer monitoring the 193.7 nm wavelength. At the end of the stirred reaction experiments ($t = 48$ h), soluble Mn was measured by inductively coupled plasma emission spectrometry (ICP-ES) at 257.610 nm.

EXAFS and Molecular Modeling Analysis. Samples of synthetic MnO_2 treated with As(III) were prepared for EXAFS analysis by reacting 1.00 g of synthetic MnO_2 with 1.0 L of 1.0 mM As(III) in 0.10 M NaCl in a stirred 2 L glass beaker for 24 h at pH 6.50. An identical preparation was made using As(V). After settling, the As(III)/As(V) speciation in the overlying solution was analyzed by HPLC−HGAAS, and the solids were collected and rinsed with DI water on ashless filter paper. The As(III)- and As(V)-treated samples were stored as wet pastes on the filter paper for 3 days prior to EXAFS analysis in sealed polycarbonate test tubes. Oxidation of As(III) was not a concern because this reaction had gone to completion in the initial sample preparation. Solutions of 1.0 mM As(III) and 1.0 mM As(V) were also analyzed to examine the X-ray absorption edge features of soluble As(III) and As(V) and background contributions to EXAFS spectra.

EXAFS and XANES spectra were collected at the Stanford Synchrotron Radiation Laboratory (SSRL) on beamline 4−3 using a Si(220) monochromator and a 13 element germanium semiconductor detector (*33*). The K edge of As (11 867 eV) was examined using an energy range of 11 667−12 867 eV, and at least 5 individual scans were collected for each sample. The XANES region of the X-ray absorption spectrum (11 860−11 900 eV) was analyzed by normalizing the fluorescence data to the edge-jump height and calculating the first derivative of the spectra.

The EXAFS data were analyzed using EXAFSPAK software (*34*). Individual scans were averaged, and the background X-ray absorbance was removed by fitting a linear polynomial equation through the pre-edge region. This was followed by fitting a spline function through the extended X-ray absorption region of the spectra (11 920−12 867 eV) to isolate the oscillations which are the result of backscattering of outgoing photoelectrons by coherent shells of atoms around the central As atom. The EXAFS spectra were normalized using a Victoreen polynomial function and transformed from eV to $Å^{-1}$ units to produce the EXAFS function ($\chi(k)$), where k ($Å^{-1}$) is the photoelectron wave vector. The $\chi(k)$ function was then weighted by k^3 and truncated leaving a k range of 3.65−15.52 $Å^{-1}$ for fitting. Fourier transformation (FT) of the k^3-weighted $\chi(k)$ function ($\chi(k)k^3$) in k space ($Å^{-1}$) yielded the radial structure function (RSF) in R space (Å), where peaks correspond to atomic shells around the As atom (e.g., As−O and As−Mn).

The theoretical EXAFS expression was fit to experimental data using EXAFSPAK. The As−O and As−Mn RSF peaks were isolated by selecting the R window at the minimum amplitude points around peaks. The As−O and As−Mn R windows were 0.988−1.618 and 2.535−3.073 Å, respectively for both As(III)- and As(V)-treated MnO_2. Peaks in the RSF were first analyzed individually, followed by analysis of a composite R window of 0.988−3.073 Å which contained both As−O and As−Mn shells. Individual As−O and As−Mn R windows and the composite As−O + As−Mn R window were back-Fourier transformed to produce the Fourier filtered EXAFS functions. Fourier filtered experimental EXAFS data were fit with a theoretical EXAFS equation in which the coordination number (N), the interatomic distance (R), the Debye−Waller term (σ^2), and the energy offset (E_0) were used as adjustable parameters to give the best fit to the Fourier filtered data. Phase and amplitude functions for the absorber and backscatterers were defined using single-scattering curved wave assumptions in the FEFF 7.0 model (*35*, *36*). Values of N, R, σ^2, and E_0 which were fitted to Fourier filtered data were then used as starting values to model the raw unfiltered EXAFS data. Error estimates of the fitted parameters were R ±0.02 Å, N ±20%, and σ^2 ±20−30%.

Molecular modeling calculations were performed on representative Mn−As−O clusters using PC Spartan Pro and perturbed Becke−Perdue density functional calculations with full numerical polarization. In most cases, the results were similar to PM3 semiempirical and 6-31G* Hartree−Fock methods. The clusters used to simulate the As(V) surface complex on MnO_2 involved the construction of a $Mn(OH)_6$ octahedron (or two for a binuclear complex) with 1, 2, or 3 of the hydroxyls replaced with an $HAsO_4^{2-}$ group. Complete

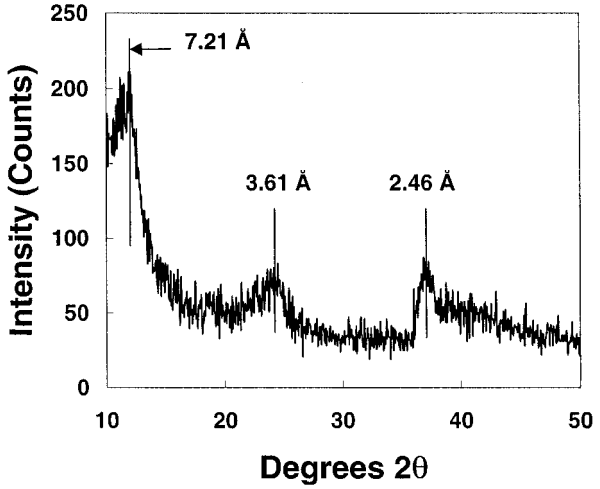

FIGURE 1. X-ray powder diffraction pattern of synthetic birnessite.

protonation of the complex was used to minimize the net charge on the complex. The oxidation state of Mn was adjusted in the calculation between Mn(II), Mn(III), and Mn(IV) by changing the total number of electrons in the system. The attachment of As(V) (e.g., monodentate vs bidentate) was also specified, and the most stable atomic configuration and interatomic distances were determined.

Results and Discussion

Synthetic MnO_2. Three dominant reflections at 2.46, 3.61, and 7.21 Å were observed in the XRD pattern (Figure 1) consistent with peaks observed for synthetic birnessite by others (*18, 21, 27*). The synthetic MnO_2 solid had a composition of 4.9% K, 50.5% Mn, 15.0% H_2O, and 29.6% O (% w/w). This composition is similar to a previous birnessite material used by Moore et al. (*18*) who investigated As(III) oxidation by synthetic birnessite which contained 1.7% and 8.2% K by weight. The MnO_2 had a specific surface area of 32.0 $m^2\ g^{-1}$, measured by BET N_2 analysis similar to the MnO_2 material reported previously (*26*).

Batch Reactor Study. The oxidation of As(III) by synthetic MnO_2 at two different solid concentrations at pH 6.50 is shown in Figure 2. Rapid uptake of As(III) by MnO_2 is apparent as well as formation of both soluble and adsorbed As(V). Dissolved As(III) was below the detection limit at 1 h in the higher (250 mg L^{-1}) MnO_2 suspension density, and approximately 30% of the original As(III) added was unrecoverable and presumed to be adsorbed As(V) (Figure 2b). At the termination of the reaction (48 h), the As surface coverage on MnO_2 achieved was 253 and 121 mmol As kg^{-1} (7.91 and 3.78 μmol m^{-2}As) in the 100 mg L^{-1} MnO_2 and 250 mg L^{-1} MnO_2 systems, respectively. Chromatograms collected from the 100 mg L^{-1} MnO_2 reaction provided direct, simultaneous speciation of As(III) and As(V) in solution (Figure 3). The As(III) solution concentration time series data were analyzed by fitting a first-order rate equation to the 0−0.5 and 0−2 h portions of the 100 mg L^{-1} MnO_2 and 250 mg L^{-1} MnO_2 systems, respectively (Figure 4). Efforts to fit first-order rate equations to the entire time series (0−48 h) were unsuccessful. Therefore, only the initial fast As(III) uptake reaction data was used for analysis. The rate of As(III) uptake at the 100 and 250 mg L^{-1} suspension densities was first-order dependent on [As(III)]; however, the slopes in Figure 4 were not proportional to suspension density. This suggested that the measured As(III) uptake reaction rate was not an elementary rate but an apparent rate which was complicated by other surface reactions such as MnO_2 surface alterations during the As(III) oxidation reaction or competition between with As(V) product for binding sites.

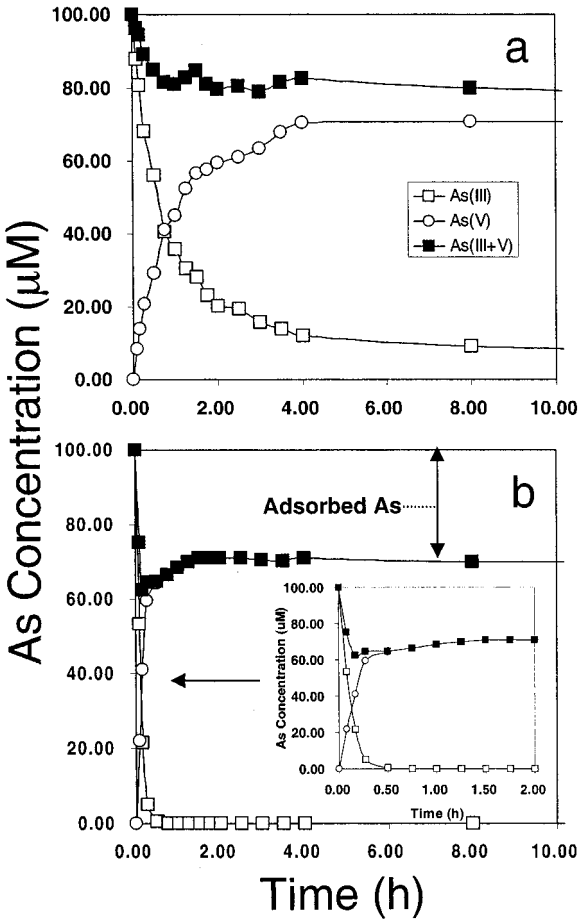

FIGURE 2. Speciation of dissolved As(III)/(V) and total As(III) + (V) recovery during the reaction of 0.10 mM As(III) with synthetic birnessite (MnO_2) as a function of time: (a) 100 mg L^{-1} MnO_2 and (b) 250 mg L^{-1} MnO_2 with inset showing expanded 0−2 h region of data.

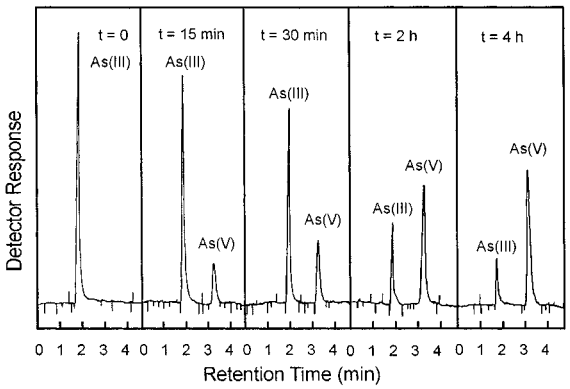

FIGURE 3. HPLC−HGAAS chromatograms showing the detection method for As(III)/(V) speciation during the 0−4 h time course of the reaction of 0.10 mM As(III) with synthetic birnessite 100 mg L^{-1} MnO_2.

The dissolved Mn^{2+} concentration was 9.09 and 5.10 μM for the 100 and 250 mg L^{-1} MnO_2 systems, respectively, showing that the production of dissolved Mn^{2+} was not stoichiometrically related to As(III) oxidation in our experiments. The nonstoichiometric relationship between As(III) oxidation and release of dissolved Mn(II) is evidence for the formation of Mn(III), which remains in the MnO_2 crystal structure as the product of a one electron-transfer reaction step (eq 2) (*19*). Other previous work, however, has found a nearly stoichiometric association between As(III) oxidation

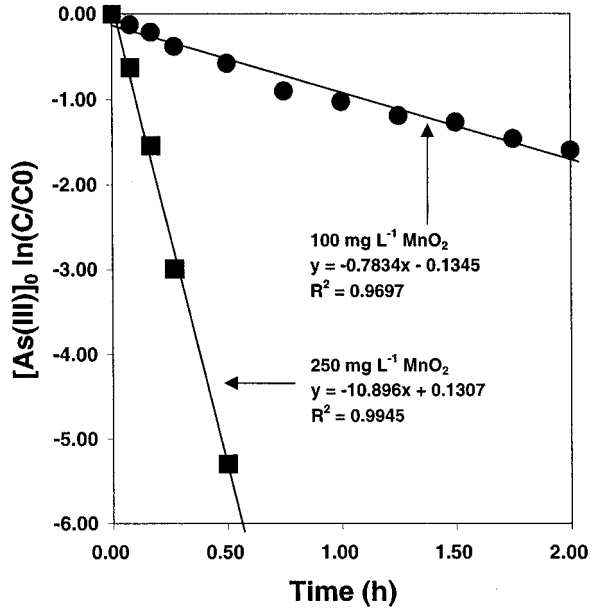

FIGURE 4. Linear regression analysis of normalized As(III) uptake by synthetic birnessite (MnO_2) at two suspension densities (100 and 250 mg L^{-1} MnO_2).

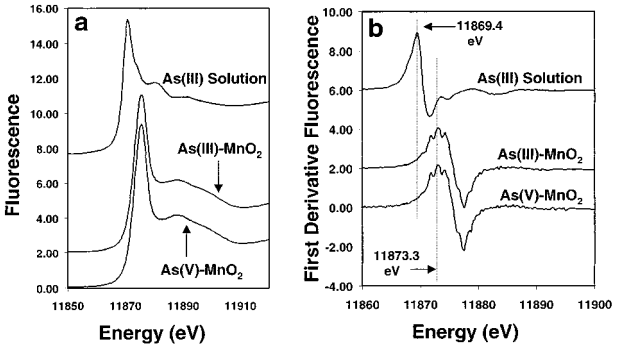

FIGURE 5. K-edge XANES spectra (a) and first derivatives of the spectra (b) for the As(III)- and As(V)-treated synthetic birnessite (MnO_2) and a solution of 1.0 mM As(III) (pH 6.5). Also shown are the maxima in the derivative curves at 11 869.4 eV (As(III)) and 11 873.3 eV (As(V)).

to As(V) and release of dissolved Mn at pH 4 (*20*). Oxidation of Cr(III) to Cr(VI) by MnO_2 at pH 3.0 and 5.0 resulted in 1.5 Mn^{2+} formed for each Cr(III) oxidized (*27*). At pH 6.50 in the present study, however, the MnO_2 particle surface contains negatively charged surface functional groups ($\equiv Mn-O^-$); thus, soluble Mn^{2+} formed by reductive dissolution of MnO_2 remains adsorbed on the negatively charged surface.

EXAFS and XANES Analysis. Synthetic MnO_2 was treated with both As(III) and As(V) for EXAFS and XANES analysis. The K-edge XANES spectra and their first derivatives for the As-treated MnO_2 and a 1.0 mM As(III) solution are shown in parts a and b of Figure 5. The K-edge data exhibit an absorption edge difference of 3.9 eV (or 1.95 eV per unit oxidation state change) between the As(III) solution and the As(III)- and As(V)-treated MnO_2 samples (Figure 5b). Noticeable differences are evident in the first derivative data for As(III) solution and As-treated MnO_2 samples, including the multiple peak pattern for As-treated MnO_2 samples. The first derivative data indicate that a nearly identical structural and electronic environment exists in the As(III)- and As(V)-treated MnO_2 samples. This is direct evidence that the As(III) oxidized by MnO_2 solids was adsorbed as As(V).

The theoretical EXAFS functions ($\chi(k)k^3$) for As(III)- and As(V)-treated MnO_2 and the 1.0 mM As(V) solution are shown

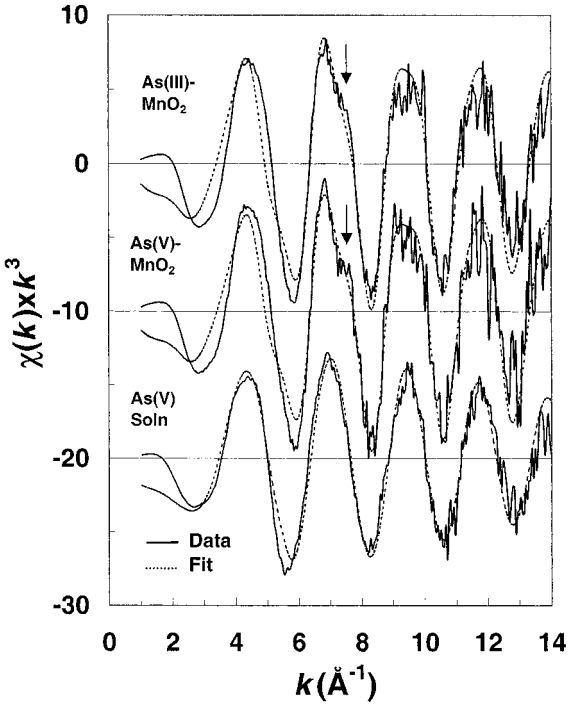

FIGURE 6. Experimental, unfiltered EXAFS data for As(III)- and As(V)-treated synthetic birnessite (MnO_2) at pH 6.5 and a solution of 1.0 mM As(V) (solid lines). Also shown is the theoretical fit (dashed lines) of the EXAFS function ($\chi(k)k^3$) which contains As−O and As−Mn shell contributions As-treated synthetic birnessite. Arrows indicate the sine wave beat-pattern contribution from the As−Mn shell.

TABLE 1. EXAFS Parameters Optimized Using EXAFSPAK for As(III)- and As(V) Treated Synthetic MnO_2 and 1.0 MM As(V) Solution

sample	shell	N^a	R (Å)	σ^2	E_0
As(III)−MnO_2	As−O	3.89	1.69	1.00×10^{-3}	−1.75
	As−Mn	2.01	3.22	6.02×10^{-3}	−1.75
As(V)−MnO_2	As−O	3.90	1.69	7.00×10^{-4}	−1.56
	As−Mn	1.99	3.22	4.95×10^{-3}	−1.56
1.0 mM As(V)	As−O	4.00	1.69	2.00×10^{-3}	0.02

[a] N = coordination number, R = interatomic distance (error = ±0.02 Å), σ^2 = Debye−Waller term, E_0 = energy offset (threshold E_0 shift in eV, used for all shells).

in Figure 6. The $\chi(k)k^3$ EXAFS expression was fit to the experimental data, and the resulting adjustable parameters (N, R, σ^2, and E_0) for As(III)- and As(V)-treated MnO_2 and the 1.0 mM As(V) solution sample are given in Table 1. The fitted lines (dotted, Figure 6) for As(III)- and As(V)-treated MnO_2 represent a composite sine wave with a primary contribution from the first shell of ~3.90 O atoms surrounding the As atom in tetrahedral symmetry (As−O shell) at an average distance of 1.69 Å. Smaller, but distinct, contributions from ~2.00 Mn atoms at 3.22 Å from the As atom are also components in the fits to As(III)- and As(V)-treated MnO_2 samples. The contribution of the second shell of Mn atoms results in a noticeable second harmonic beat (arrows, Figure 6) in the EXAFS data.

The As−O interatomic distance was 1.69 Å for both As(III)- and As(V)-treated MnO_2 samples, which was 0.01−0.02 Å greater than previously reported As−O interatomic distances for As(V) (*37*−*39*) but shorter than the 1.78−1.79 Å reported for As(III) (*37*, *40*). Both As(III)- and As(V)-treated MnO_2 samples were best described with an As−Mn shell at 3.22 Å (Table 1). The Fourier transform of the data in Figure 6

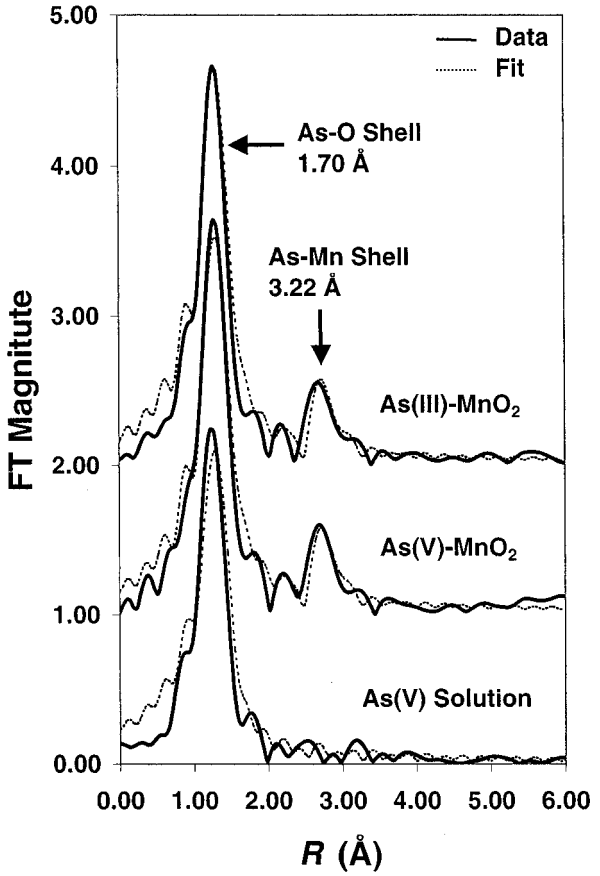

FIGURE 7. Radial structure functions (not phase corrected) for As(III)- and As(V)-treated synthetic birnessite (MnO_2) and 1.0 mM As(V) solution. Dashed lines are the fits to the experimental RSF data and peaks correspond to As−O and As−Mn atomic shells around the As atom.

resulted in a distinct second shell peak in the radial structure functions (RSF) (Figure 7). The RSF data in Figure 7 were not phase-corrected and appear shifted slightly (about −0.45 Å) from interatomic distances fit by EXAFSPAK and in Table 1. The As(V) solution RSF gives an indication of As(V) which is not bound to the MnO_2 solid phase with no As−Mn shell included in the fit. The As−Mn distance of 3.22 Å is characteristic of double-corner sharing polyhedra, consistent with surface complexes of As(V) noted for Fe (hydr)oxides (*38*).

To help constrain As−Mn interatomic distances and identify the most likely oxidation state of Mn to which As(V) is complexed, molecular modeling calculations were applied to hypothetical As−Mn clusters. Previous investigations have speculated that As(III)-treated birnessite may produce an Mn(II)−As(V) solid phase of the form $Mn_3(AsO_4)_2$ (*18*). Because of the increased ionic radius of the Mn(II) ion, longer As−Mn interatomic distances were calculated than were observed with EXAFS. For example, the As−Mn distance in a hypothetical Mn(II)-containing $Mn_2(OH)_8(AsO_4)^{7-}$ cluster was 3.48 Å, which is 0.26 Å longer than that observed by EXAFS. This narrows the As(V) product to a surface complex with either Mn(IV) or Mn(III) or some combination of these polyhedra. On the basis of this information, in combination with the fact that the exact same EXAFS-derived As−Mn interatomic distance was found for both As(III)- and As(V)-treated MnO_2 samples, it appears that As(V), either added as As(V) or formed from oxidation of As(III), results in a surface complex on predominantly Mn(IV) polyhedra within birnessite. The hypothetical Mn(IV)-containing clusters, including monodentate mononuclear ($Mn(OH)_5(HAsO_4)^{3-}$) and bidentate binuclear ($Mn_2(OH)_8(AsO_4)^{3-}$), yielded As−Mn distances which were more consistent with the EXAFS results.

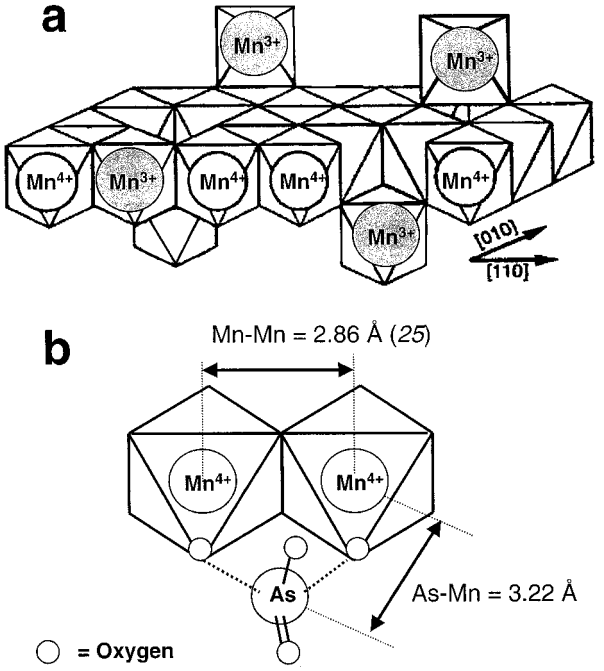

FIGURE 8. Structural diagram of MnO_2 crystallite corresponding to 7 Å manganate (a) (adapted from Manceau et al. (*25*)) and possible linkages between an arsenate ion (As(V) tetrahedron) and a pair of edge-linked MnO_6 octahedra (b). As−Mn interatomic distance was was 3.22 Å, suggesting a bidentate binuclear complex.

On the basis of our results, a structural diagram of the most likely As(V) complex was developed (Figure 8). A birnessite crystallite showing linked Mn(III) and Mn(IV) octahedra and octahedral "holes" developed according to previously determined birnessite crystal structures (*25*, *30*) is also included (Figure 8a). The proposed bidentate As(V) tetrahedron attachment mechanism to the birnessite crystal structure is supported experimentally by the presence of the As−Mn backscattering peak from a shell of Mn atoms at 3.22 Å for both As(III)- and As(V)-treated MnO_2. When As(V) is reacted with Fe hydroxides (goethite or ferrihydrite), the predominant As(V)−Fe interatomic distances measured by EXAFS are between 3.24 and 3.28 Å (*38*, *39*), indicative of a bidentate bridged complex linking adjacent apexes of two edge-sharing Fe octahedra. Considering the slightly smaller ionic radius of Mn(IV) (0.60 Å) compared with Fe(III) (0.64 Å) (*41*), our results are consistent with previously proposed As−Fe interatomic distances for As(V) complex formation on Fe oxides (*38*, *39*).

Surface Coverage and Mn(II) Dissolution. Surface coverages achieved for As(III)- and As(V)-treated synthetic MnO_2 were 266 and 50.7 mmol kg^{-1} As (8.79 and 1.67 μmol m^{-2} As), respectively. The As(III)-treated MnO_2 sample analyzed by EXAFS had a comparable surface coverage to the 100 mg L^{-1} MnO_2 batch reaction (7.91 μmol m^{-2} As). The dramatic difference in As surface coverage between the As(III)- and As(V)-treated MnO_2 samples was caused by As(III)-induced surface alteration during reductive dissolution of MnO_2. Oscarson et al. (*23*) found that As(III) oxidation rate increased and reached a maximum as the amount of As(III) was increased at a fixed MnO_2 suspension density. It was postulated that a barrier was formed at or near the surface of the oxide that prevented further reduction of the structural Mn(IV) in the interior of crystallites (*23*). This is consistent with our results, which suggest that a surface layer of covalently bound As(V) forms on the reacted MnO_2 surface which would limit further reaction of MnO_2 with As(III).

Dissolution of synthetic MnO_2 by As(III) (*18*−*21*) and Cr(III) (*27*) releases Mn^{2+} ions, making fresh adsorption sites for As(V). XPS studies (*19*) also suggest the formation of Mn(III) from reductive dissolution of MnO_2 during As(III) oxidation, allowing for the possible formation of MnOOH*−As(V) complexes.

The results of this investigation confirm the work of previous investigators who found that the reaction of As(III) with MnO_2 results in As(III) oxidation to As(V). Though we have not addressed the initial formation of an As(III)−MnO_2 complex prior to oxidation in this study, presumably the As(III) species also forms an inner-sphere complex on MnO_2 followed by electron transfer from As(III) to Mn(VI) and release of As(V) and Mn(II). The majority of As(V) formed is released to the solution, with a significant fraction (between 20% and 30% depending on suspension density) being adsorbed on the MnO_2 surface. The EXAFS results confirm that the As(V) surface complex on both the As(III)-altered MnO_2 and unaltered MnO_2 surfaces is an inner-sphere bidentate binuclear complex with an As−Mn interatomic distance of 3.22 Å. This research suggests that MnO_2 materials used at near neutral pH in environmental remediation or drinking water filtering would play a beneficial role as both an efficient oxidant of As(III) and a sorbent for As(V).

Acknowledgments

This research was supported by the U.S. Department of Agriculture National Research Initiative Competitive Grants Program (Project No. 9604171).

Literature Cited

(1) Arsenic contamination of groundwater and its remedial action plan in West Bengal. AIIH&PH. In *Consultation on arsenic in drinking water and resulting arsenic toxicity in India and Bangladesh*; World Health Organization: New Delhi, India, 1997.
(2) Dhar, R. K.; Biswas, B. K.; Samanta, G.; Mandal, B. K.; Chakraborti, D.; Roy, S.; Jafar, A.; Islam, A.; Ara, G.; Kabir, S.; Khan, A. W.; Ahmed, S. A.; Hadi, S. A. *Curr. Sci.* **1997**, *73*, 48−59.
(3) Bhattacharya, P.; Chatterjee, D.; Jacks, G. *Int. J. Water Res. Manage.* **1997**, *13*, 79−92.
(4) Aurilio, A. C.; Mason, R. P.; Hemond, H. F. *Environ. Sci. Technol.* **1994**, *28*, 577−585.
(5) Hansen, S. H.; Larsen, E. H.; Pritzl, G.; Cornatt, C. *J. Anal. At. Spectrom.* **1992**, *7*, 629−634.
(6) Masscheleyn, P. H.; Delaune, R. D.; Patrick, W. H., Jr. *J. Environ. Qual.* **1991**, *20*, 522−527.
(7) Tye, C. T.; Haswell, S. J.; O'Neil, P.; Bancroft, K. C. C. *Anal. Chim. Acta* **1985**, *169*, 195−200.
(8) Sadiq, M.; Zaida, T. H.; Mian, A. A. *Water, Air, Soil Pollut.* **1983**, *20*, 369−377.
(9) Korte, N. E.; Fernando, Q. *Crit. Rev. Environ. Control* **1991**, *21*, 1−39.
(10) Cherry, J. A.; Shaikh, A. U.; Tallman, D. E.; Nicholson, R. V. *J. Hydrol.* **1979**, *43*, 373−392.
(11) Ferguson, J. F.; Gavis, J. *Water Res.* **1972**, *6*, 1259−1274.
(12) Knowles, F. C.; Benson, A. A. *Trends Biochem. Sci.* **1983**, *8*, 178−180.
(13) Coddington, K. *Toxicol. Environ. Chem.* **1986**, *11*, 281−290.
(14) Manning, B. A.; Goldberg, S. *Environ. Sci. Technol.* **1997**, *31*, 2005−2011.
(15) Manning, B. A.; Goldberg, S. *Soil Sci.* **1997**, *162*, 886−895.
(16) Manning, B. A.; Suarez, D. L. *Soil Sci. Soc. Am. J.* **2000**, *64*, 128−137.
(17) Foster, A. L.; Brown, G. E., Jr.; Parks, G. A. *Environ. Sci. Technol.* **1998**, *32*, 1444−1452.
(18) Moore, J. N.; Walker, J. R.; Hayes, T. H. *Clays Clay Miner.* **1990**, *38*, 549−555.
(19) Nesbitt, H. W.; Canning, G. W.; Bancroft, G. M. *Geochim. Cosmochim. Acta* **1998**, *62*, 2097−2110.
(20) Scott, M. J.; Morgan, J. J. *Environ. Sci. Technol.* **1995**, *29*, 1898−1905.
(21) Oscarson, D. W.; Huang, P. M.; Liaw, W. K.; Hammer, U. T. *Soil Sci. Soc. Am. J.* **1983**, *47*, 644−648.
(22) Scott, M. J. Ph.D. Thesis, California Institute of Technology, Pasadena, CA, 1991.
(23) Oscarson, D. W.; Huang, P. M.; Liaw, W. K. *Clays Clay Miner.* **1981**, *29*, 219−225.
(24) Oscarson, D. W.; Huang, P. M.; Liaw, W. K. *J. Environ. Qual.* **1980**, *9*, 700−703.
(25) Manceau, A.; Drits, V. A.; Silvester, E.; Bartoli, C.; Lanson, B. Structural mechanism of Co^{2+} oxidation by the phyllomanganate buserite. *Am. Mineral.* **1997**, *82*, 1150−1175.
(26) McKenzie, R. M. *Aust. J. Soil Res.* **1970**, *8*, 97−106.
(27) Fendorf, S. E.; Zasoski, R. J. *Environ. Sci. Technol.* **1992**, *26*, 79−85.
(28) McBride, M. B. *Soil Sci. Soc. Am. J.* **1987**, *51*, 1466−1472.
(29) Stone, A. T. In *Rates of Soil Chemical Processes*; Sparks, D. L., Suarez, D. L., Eds.; SSSA Special Publication: Madison, WI, 1991.
(30) Drits, V. A.; Silvester, E.; Gorshkov, A. I.; Manceau, A. *Am. Mineral.* **1997**, *82*, 946−961.
(31) Silvester, E.; Manceau, A.; Drits, V. A. *Am. Mineral.* **1997**, *82*, 962−978.
(32) Manning, B. A.; Martens, D. A. *Environ. Sci. Technol.* **1997**, *31*, 171−177.
(33) Cramer, S. P.; Tench, O.; Yocum, M.; George, G. N. *Nucl. Instrum. Methods Phys. Res., Sect. A* **1988**, *266*, 586−591.
(34) George, G. N.; Pickering, I. J. *EXAFSPAK: A Suite of Computer Programs for Analysis of X-ray Absorption Spectra*. Stanford Synchrotron Radiation Laboratory: Stanford, CA, 1993.
(35) Mustre de Leon, J.; Rehr, J. J.; Zabinsky, S. I.; Albers, R. C. *Phys. Rev. B: Condens. Matter* **1991**, *44*, 4146−4149.
(36) Rehr, J. J.; Mustre de Leon, J.; Zabinsky, S. I.; Albers, R. C. *J. Am. Chem. Soc.* **1991**, *113*, 5135−5140.
(37) Foster, A. L.; Brown, G. E., Jr.; Tingle, T. N.; Parks, G. A. *Am. Mineral.* **1998**, *83*, 553−568.
(38) Waychunas, G. A.; Rea, B. A.; Fuller, C. C.; Davis, J. A. *Geochim. Cosmochim. Acta* **1993**, *57*, 2251−2269.
(39) Fendorf, S.; Eick, M. J.; Grossl, P.; Sparks, D. L. *Environ. Sci. Technol.* **1997**, *31*, 315−320.
(40) Manning, B. A.; Fendorf, S. E.; Goldberg, S. *Environ. Sci. Technol.* **1998**, *32*, 2383−2388.
(41) *Handbook of Chemistry and Physics*, 72nd ed.; Lide, Ed.; Chemical Rubber Company: Boca Raton, FL, 1991; p 12-8.

Received for review May 30, 2001. Revised manuscript received December 7, 2001. Accepted December 13, 2001.

ES0110170